ARTICLE

Enhancement of Active Corrosion Protection via Combination of Inhibitor-Loaded Nanocontainers

J. Tedim,*,† S. K. Poznyak,† A. Kuznetsova,† D. Raps,‡ T. Hack,‡ M. L. Zheludkevich,† and M. G. S. Ferreira†,§

Department of Ceramics and Glass Engineering, CICECO, University of Aveiro, 3810-193 Aveiro, Portugal, EADS Innovation Works, 81663 Munich, Germany, and IST, ICEMS, Technical University of Lisbon, Avenida Rovisco Pais, 1049-001 Lisbon, Portugal

ABSTRACT The present work reports the synthesis of layered double hydroxides (LDHs) nanocontainers loaded with different corrosion inhibitors (vanadate, phosphate, and 2-mercaptobenzothiazolate) and the characterization of the resulting pigments by X-ray diffraction (XRD) and transmission electron microscopy (TEM). The anticorrosion activity of these nanocontainers with respect to aluminum alloy AA2024 was investigated by electrochemical impedance spectroscopy (EIS). The bare metallic substrates were immersed in dispersions of nanocontainers in sodium chloride solution and tested to understand the inhibition mechanisms and efficiency. The nanocontainers were also incorporated into commercial coatings used for aeronautical applications to study the active corrosion protection properties in systems of industrial relevance. The results show that an enhancement of the active protection effect can be reached when nanocontainers loaded with different inhibitors are combined in the same protective coating system.

KEYWORDS: nanocontainer • coating • corrosion • inhibitor • self-healing • AA2024

INTRODUCTION

Nowadays, the most widespread approach for corrosion protection of metallic substrates is the application of protective polymer coatings. The main role of an anticorrosion coating is to protect the metal, acting as an effective barrier against corrosive species present in the environment. Natural polymer aging and external destructive impacts like UV radiation, temperature gradients, mechanical stresses, or presence of aggressive chemicals lead to the formation of micropores and microcracks that interrupt the barrier effect and allow the direct ingress of corrosive species into the metal surface (1). Once corrosion started, the polymer coating no longer protects the defective zone and paint creepage is initiated at the defect. Thus, it is necessary to impart self-healing functionalities to coatings, i.e., the ability to repair the defects in an autonomous way and provide long-term protection.

The term "self-healing" can be defined as the ability of a material to recover its initial properties after destructive action by external agents or under the influence of internal stresses. In Nature, a damage inflicted to an organism evokes a healing response (2−4). Such examples have inspired material designers to combine traditional engineering approaches with biological self-healing mechanisms. Many academic and industrial groups are currently exploring new strategies to obtain self-repairing materials. However, the number of commercialized systems showing this capability is still limited. When applied to protective coatings, this concept has been interpreted in different ways (5). In the case of corrosion, the self-recovering ability has been considered in a more restricted form because the main function of coatings is to protect metallic substrates against an environmentally induced corrosion attack. Therefore, the restoration of all the coating functionalities is not obligatory as long as the corrosion activity is hindered. This can be achieved by direct incorporation of corrosion inhibitors into coating formulations, in order to confer active protection when the coating barrier properties fail (6, 7).

Chromate-derived species were the most effective inhibitors used in the past. Nonetheless, their high toxicity and carcinogenic nature lead to the creation of strict environmental regulations. As a result, the utilization of these species has been prohibited in the EU since 2007, but a truly replacement for chromates has not been found yet. There are no reports of single species with a inhibiting performance superior or at least comparable to those of Cr(VI) species. One possibility to outperform chromates is to use combinations of inhibitors. There are some reports of synergistic combination of inhibitors for steel (8, 9), copper (10), and aluminum alloy (11−13) substrates. At the same time, new screening methodologies based on electrochemical techniques are being developed to allow fast monitoring of different inhibitors in different conditions (concentration, pH) and hence provide new synergistic systems in a relatively short time. These include the high-throughput screening methods based on DC polarization tests developed by

* Corresponding author. E-mail: joao.tedim@ua.pt.
Received for review March 2, 2010 and accepted April 27, 2010
† University of Aveiro.
‡ EADS Innovation Works.
§ Technical University of Lisbon.
DOI: 10.1021/am100174t

Published on Web 05/10/2010

Scheme 1. Schematic View of the LDHs Action in Corrosion Protection[a]

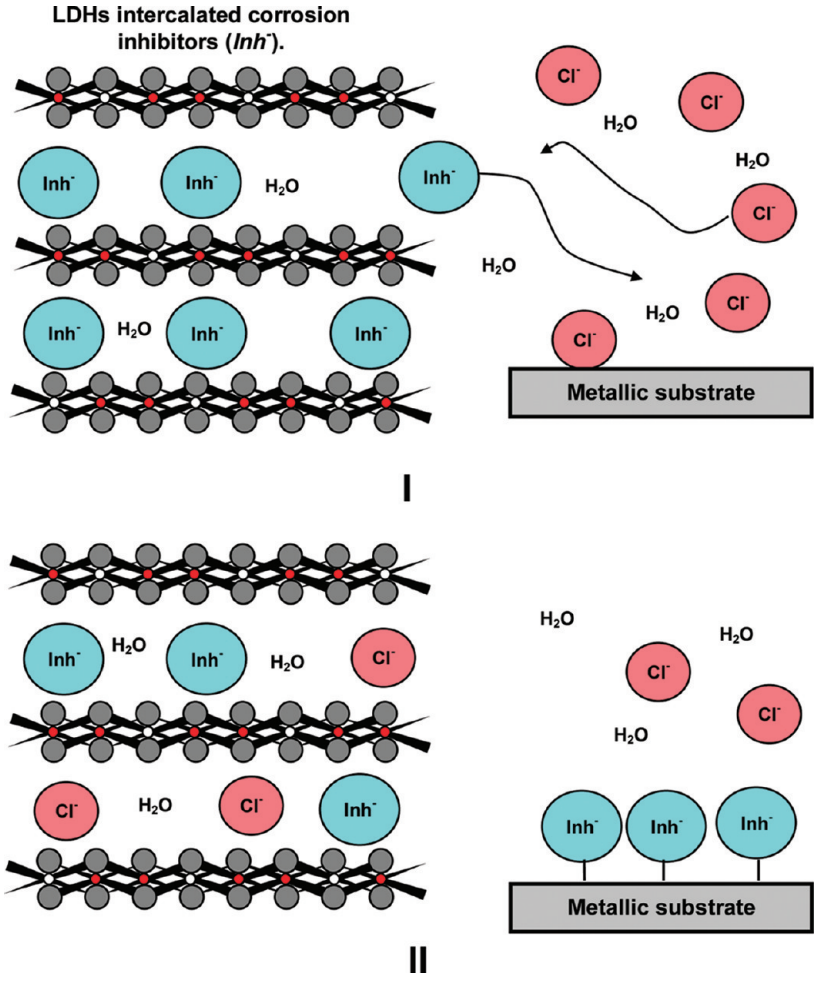

[a] (**I**) The release of inhibitors (**Inh**$^-$) is triggered by the presence of anions in solution (**Cl**$^-$). (**II**) LDHs play a double-role, providing inhibitors to protect the metallic substrates and entrapping aggressive species from the environment.

Chambers and co-workers (14), its adaptation for multielectrode measurements by Muster and colleagues (15), and the multielectrode cell developed for the scanning vibrating electrode technique (SVET) by Kallip and colleagues (16).

If the inhibiting species are directly incorporated into coatings, detrimental interactions may occur between the matrix and the active species, namely the loss of the inhibition capability, coating degradation or both (17). A promising strategy to overcome this problem is the encapsulation of inhibitors within inert host structures of nanometer dimensions, referred hereafter as nanocontainers. These nanostructured materials will store the inhibitors while the coating is able to maintain the metallic substrate protected (barrier effect). Upon breakdown of the coating barrier properties, active species are released to inhibit the corrosion processes (18). Among the multitude of reported nanocontainers are cyclodextrins (19, 20), oxide nanoparticles (21), and polymeric layer-by-layer (LbL) assembled shells (22−25).

Anion-exchange pigments can also be used to immobilize anionic inhibitors (18, 26−29). In this case, the release of anionic inhibitors is triggered by anion-exchange with corrosion aggressive chloride ions, thereby playing a double role: entrapment of harmful chlorides and release of inhibitors. Layered double hydroxides (LDHs) are anion-exchange systems consisting of stacks of positively charged, mixed-metal hydroxide layers, between which anionic species and solvent molecules are intercalated (Scheme 1) (30). They have been applied in a wide range of areas including catalysis (31) and drug-delivery systems (32).

In corrosion science and engineering, several groups have tested LDHs as containers for corrosion inhibitors, including Buchheit's (27, 28), McMurray's (33), and Kendig's (34). Recently, our group has reported the synthesis and characterization of LDHs intercalated with organic anions and divanadates (35, 36). These layered materials were shown to inhibit corrosion on AA20204 substrates, when added to the electrolyte (35, 36) and when incorporated into protective coatings (36). Having proved the inhibition effect provided by inhibitor-loaded nanocontainers, there are some technical obstacles yet to be overcome, namely the (low) concentration of corrosion inhibitors within the coating formulations. Nanocontainers are not soluble and can only be added to coating formulations up to a certain concentration limit, above which agglomeration effects and/or deterioration of coating barrier properties occur. This could be solved, at least to some extent, by conjugation of different

factors: inhibitor strength, mechanism and extent of inhibitor release from the nanocontainers, and combination of inhibitors that provide synergistic effects.

In this study, we report the synergistic effect on corrosion protection of AA2024 that results from the combination of LDH nanocontainers intercalated with different inhibiting anions, namely vanadate (VO_x), phosphate (H_xPO_4), and 2-mercaptobenzothiazolate (MBT). The protective effect provided by mixed LDHs was investigated on bare AA2024 substrates immersed in LDH-containing electrolyte solutions and on substrates covered with LDH-doped protective coatings.

MATERIALS AND METHODS

Materials. All the chemicals were obtained from Aldrich, Fluka, and Riedel-de Häen, with ≥98% of ground substance, and used as received.

Synthesis of Layered Double Hydroxides Intercalated with Inhibitors. Zn−Al LDHs were prepared by the ion-exchange method. Accordingly, nitrate anions intercalated in the preformed LDHs (first step) are replaced by anionic corrosion inhibitors via an anion-exchange reaction (second step) (35, 36). The synthesis was carried out under argon atmosphere and all the solutions were prepared using boiled distilled water, in order to avoid contamination with carbonate anions. The Zn:Al ratio chosen for the synthesis was 2:1 to obtain stable layered compounds. In the first step, a 0.5 M Zn $(NO_3)_2 \times 6H_2O$ and 0.25 M $Al(NO_3)_3 \times 9H_2O$ solution ($V = 50$ mL) was slowly added to 1.5 M $NaNO_3$ ($V = 100$ mL, pH 10) under vigorous stirring at room temperature (the addition took approximately 1.5 h). During this reaction, the pH was kept constant (pH 10 ± 0.5) by simultaneous addition of 2 M NaOH. Afterward, the obtained slurry was subjected to thermal treatment at 65 °C for 24 h for crystallization of the LDHs, and consequently centrifuged and washed 4 times with boiled distilled water. A small fraction of LDHs was dried at 50 °C for XRD and TEM analysis, whereas the remnant was used in the anion-exchange reaction for replacement of nitrate by vanadate, phosphate, and MBT.

For the anion-exchange reaction (second step), a 0.1 M NaX (X = $H_2PO_4^-/HPO_4^{2-}$, VO_3^-, MBT) aqueous solution was prepared and split into two portions. NaMBT was prepared by neutralization of an aqueous solution of 2-mercaptobenzothiazole with equivalent amounts of NaOH (final pH 10.0). The deprotonation of 2-mercaptobenzothiazole in basic conditions is important for its successful intercalation in the LDHs; the anionic form is the one involved in the exchange reaction with nitrates. At the same time, MBT anion is much more soluble in aqueous solution than the uncharged molecule, which can lead to higher loadings of corrosion inhibitor in the LDHs. The pH of phosphate- and vanadate-containing solutions was adjusted to 7.0 and 8.4, respectively, using 0.1 M NaOH. The precursor LDH-NO_3 was added to the first portion of NaX solution and the suspension was held at room temperature and constant stirring for 24 h. The reaction product was then centrifuged and washed as described above for the parent LDH-NO_3. Subsequently, the second portion of inhibitor-containing solution was added to the precipitate and the procedure of anion exchange was repeated. Finally, the anion-loaded LDH powders were washed and centrifuged 4 times with boiled distilled water, frozen, and then dried by lyophilization at −78 °C.

Coating and Substrate Preparation. Before immersion tests, aluminum alloy 2024 substrates were cleaned and etched according to the following procedure: alkaline cleaning in Metaclean T2001 at 68 °C for 25 min, alkaline etching in Turco Liquid Aluminetch N2 at 60 °C for 45 s, and acid etching in Turco Liquid Smutgo NC at 30 °C for 7 min, each followed by washing in distilled water.

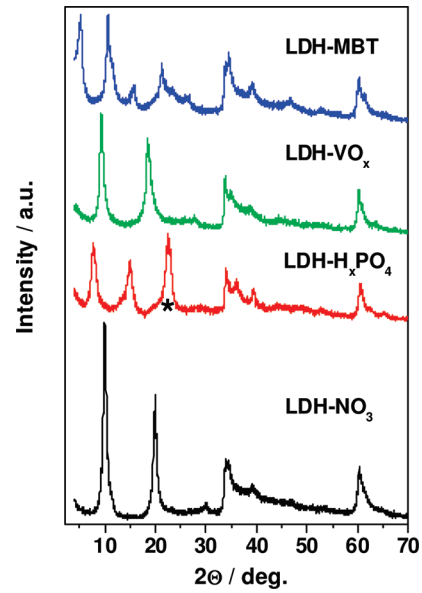

FIGURE 1. X-ray diffractograms of LDHs intercalated with nitrate (LDH-NO_3), phosphate (LDH-H_xPO_4), vanadate (LDH-VO_x), and 2-mercaptobenziothiazolate (LDH-MBT) anions; (*) denotes a non-LDH phase.

For testing of protective coatings, the cleaned aluminum substrates were coated with a thin hybrid sol−gel layer (2 μm) (pretreatment) and then overpainted with water-based epoxy paints. The hybrid sol−gel formulation was synthesized and applied as described in detail elsewhere (21). The paints used in this study were a noninhibited water-based epoxy primer (Mankiewicz SEEVENAX, thickness 25 μm) and a water-based epoxy topcoat (thickness 30 μm). Both primer and sol−gel formulations were loaded with 10% wt of the LDH nanocontainers in dry paint film. The paints were sprayed with a Sata Jet 2000 HVLP Digital spray pistol using 4.5 bar on a 1.3 spray valve and mixed with curing agents according to the technical data sheets. After applying the primer system, the top coat was deposited within the following 24 h. The coated samples were then stored at room temperature for 72 h before tests were carried out.

Examination Methods. The structure of the LDH powders was studied by X-ray diffraction (XRD) (Philips X'Pert diffractometer (Cu K_α radiation)). Particle morphology and composition were characterized by transmission electron microscopy (TEM) (Hitachi H9000 TEM, electron beam energy of 300 kV).

EIS measurements were carried out on bare alloy and coated samples at room temperature in a three-electrode cell consisting of a saturated calomel reference electrode, a platinum foil counter electrode and an AA2024 sample as working electrode in the horizontal position (exposed area of ca. 3 cm^2). The cell was placed in a Faraday cage to avoid the interference of external electromagnetic fields. The electrolyte was 0.05 M NaCl aqueous solution (10 mL), stagnant and in equilibrium with air. The measurements were performed using a Gamry FAS2 Femtostat with PCI4 Controller. The selected frequency range was from 1×10^5 to 2×10^{-3} Hz, with a 10 mV of sinusoidal perturbation. All the spectra were recorded at open circuit potential. The impedance plots were fitted using different equivalent circuits with the Echem Analyst software package from Gamry.

RESULTS AND DISCUSSION

Characterization of LDH Nanocontainers. The structure of LDHs before and after anion exchange was characterized using X-ray diffraction (Figure 1). The XRD

pattern obtained for the LDH precursors (loaded with NO_3^- anions) indicate a single-phase structure, with well-defined peaks at $2\Theta = 9.86$, 19.92, and 30.00°. These signals correspond to reflection by planes (003), (006), and (009). The gallery height can be calculated by subtracting the thickness of the cationic sheets to the basal spacing *d*. The former is approximated to the thickness of brucite layer (30), 0.477 nm, whereas the later is obtained from the position of (003) reflection, which in the case of LDH-NO_3 corresponds to a *d*-spacing of 0.90 nm. This yields a gallery height of 0.42 nm, slightly higher than the diameter of NO_3^- anion (0.38 nm) and can be ascribed to the vertical alignment of NO_3^- planar groups with respect to the host layer. Following anion exchange, there is a displacement in the position of peaks toward low 2Θ angles, accompanied by decrease in intensity (35−37). The observed peak position changes are associated with an increase in the basal spacing: 0.94 nm (LDH-VO_x), 1.14 nm (LDH-H_xPO_4), and 1.72 nm (LDH-MBT). Moreover, the absence of residual reflections assigned to the nitrate-containing LDHs guarantees the complete replacement of intercalating anions.

The pH of the vanadate-containing solution used for the anion-exchange was 8.4. In these conditions, the predominant oligovanadate species in the reaction mixture are $V_2O_7^{4-}$ and $HV_2O_7^{3-}$. The expected gallery heights of LDHs intercalated with $V_2O_7^{4-}$ are 0.78 and 0.50 nm, depending on whether the anion assumes perpendicular or parallel arrangements, respectively (38). In the present study, the gallery height determined for LDH-VO_x is 0.46 nm, suggesting that the parallel configuration is the most likely (36). For the exchange reaction with phosphate-containing solution the pH was fixed at 7.0. At this pH, $H_2PO_4^-$ and HPO_4^{2-} are the predominant species. The obtained basal spacing of LDH-H_xPO_4 is situated between the values reported by Badredine and colleagues for Zn−Al LDHs intercalated with $H_2PO_4^-$ (1.19 nm) and HPO_4^{2-} (1.06 nm) (39). Moreover, there is an additional phase (peak marked with asterisk) that may be attributed to a zinc hydrated salt. In the case of NaMBT solution used in the anion-exchange step, the pH was 10.0 to ensure the predominance of MBT anions, and thus the completion of anion substitution. The basal spacing obtained for LDH-MBT is considerably higher than that observed for LDH-VO_x and LDH-H_xPO_4 species, which is consistent with the relative size of the intercalating anions. Furthermore, the splitting and broadening of peaks found in LDH-MBT X-ray diffractogram are associated with the formation of a second LDH phase in which the MBT anion assumes a different arrangement. These findings were discussed in detail in our previous paper (35).

Figure 2 depicts TEM images of LDH-NO_3 and LDH-VO_x powders. The LDHs exhibit a plate-like morphology that is retained upon anion-exchange (panel a, b) and is in agreement with previous works (37, 40). However, particle size and agglomeration patterns seem to differ depending on the intercalating anion. At higher magnifications (panels c and d), it is possible to observe nanoparticles with hexagonal shape, which seems more regular before anion exchange.

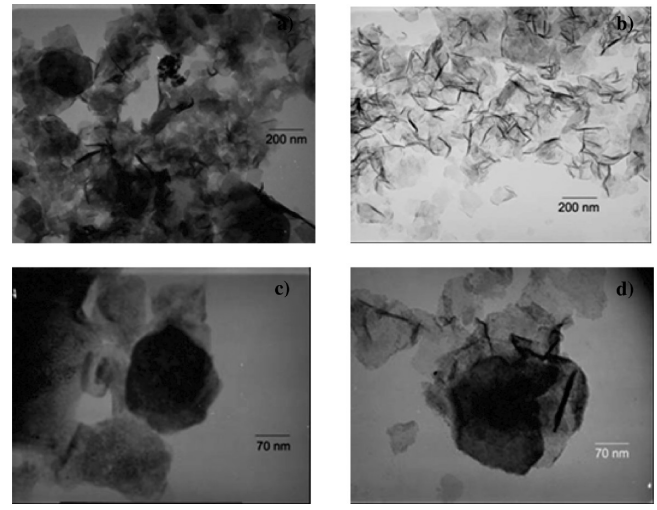

FIGURE 2. TEM images of (a, c) LDH-NO_3 and (b, d) LDH-VO_x.

The particle diameter is on the order of 200−400 nm and lateral size 20−40 nm.

The analysis of structure and morphology of the obtained LDHs clearly demonstrates that the layered structure is retained after the replacement of anions. Likewise, the release of anionic inhibitors occurs by exchange with anions available in the surroundings as demonstrated in previous papers (35, 36), and not by uncontrollable leaching/diffusion. This fact is very important when such systems are to be applied in corrosion protection: the inhibitor can be delivered on demand when corrosive anions such as chlorides are present in the environment (Scheme 1). In this way, the active protection action is triggered by the aggressiveness of the corrosive environment.

Anticorrosion Efficiency of the Inhibitor-Loaded LDH Nanocontainers. The corrosion inhibiting properties of the synthesized LDH nanocontainers with respect to aluminum alloy 2024 were assessed by electrochemical impedance spectroscopy and visual inspection of the metallic substrates during the immersion tests. In these experiments the metallic substrates were immersed in 0.05 M NaCl solutions containing the LDH powders intercalated with VO_x, H_xPO_4, and MBT anions. The total concentration of LDHs in electrolyte was 5 g L^{-1} (in the case of binary systems LDH-H_xPO_4/LDH-VO_x and LDH-MBT/LDH-VO_x, the concentration of each component was 2.5 g L^{-1}).

The optical photographs of AA2024 plates after 15 days of immersion in different solutions are depicted in Figure 3. In LDH-free electrolyte (0.05 M NaCl, panel a), the alloy surface is extensively attacked by corrosion processes, showing large corrosion pittings and deposits of white corrosion products. In the presence of LDH-H_xPO_4 (panel b), the situation improves with only a few well-defined corrosion attacks being detected, accompanied by deposition of corrosion products (white spots). In the case of LDH-MBT (panel c), two distinct regions are observed. Region A shows a shiny surface that corresponds to the place where LDH powders were deposited during the test. In contrast, region B is covered by a dense thick film, corresponding to a mixture of MBT anions and corrosion products. Similar observations

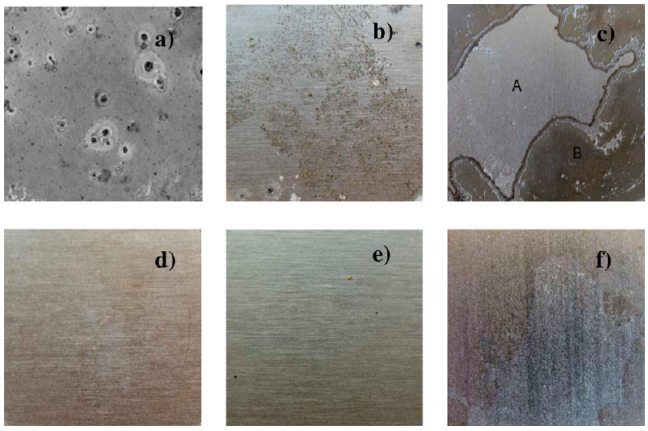

FIGURE 3. Optical photos of the AA2024 surface after 15 days of immersion in (a) 0.05 M NaCl, and 0.05 M NaCl doped with (b) LDH-H_xPO_4, (c) LDH-MBT, (d) LDH-VO_x, (e) LDH-H_xPO_4/LDH-VO_x, and (f) LDH-MBT/LDH-VO_x.

were found previously (35). The degree of corrosion of AA2024 clearly decreases in the presence of LDH-VO_x (panel d), as no corrosion pittings are detected. Instead, the presence of a film can be inferred from the darkening of the surface.

Interestingly, the best results were found for combinations of LDHs. For the LDH-H_xPO_4/LDH-VO_x system (panel e), the AA2024 surface seems slightly changed, upon which only very small defects covered with dense deposits can be detected. These places may correspond to passivated pits. Similar results were also found for the AA2024 specimen immersed in electrolyte with LDH-MBT/LDH-VO_x (panel f). In the latter case corrosion products and passivated pits are absent and only some yellowish areas are detected, probably because of the formation of protective films with MBT and VO_x.

Visual analysis of the metallic substrates already indicates a positive effect in using combinations of different nanocontainer/inhibitor systems. EIS measurements were additionally performed to study kinetics of corrosion and inhibition processes in the presence of LDH nanocontainers. Figure 4 depicts the impedance spectra after 2 days of immersion. The values of impedance modulus at low frequencies show that the LDH nanocontainers intercalated with inhibitor provides protection when compared to the background electrolyte. Among the single-type LDH systems, the impedance decreases in the following order: $|Z|$ (LDH-VO_x) > $|Z|$ (LDH-MBT) > $|Z|$ (LDH-H_xPO_4). This is in agreement with the inhibiting efficiency demonstrated by different inhibitors when available in solution. Vanadate is amidst the best corrosion inhibitors for AA2024 (27, 36); 2-mercaptobenzothiazole is also a very effective inhibitor for AA2024 in neutral form but in the present study it was used in a less-inhibiting, deprotonated form. (In a recent paper, we showed that the inhibiting efficiency of 2-mercaptobenzothiazole depends on the pH, being the best in neutral conditions (35).) Phosphate is the least efficient inhibitor for protection of AA2024 used in this work.

Two well-defined time constants can be identified in the spectra acquired for AA2024 in the electrolytes containing

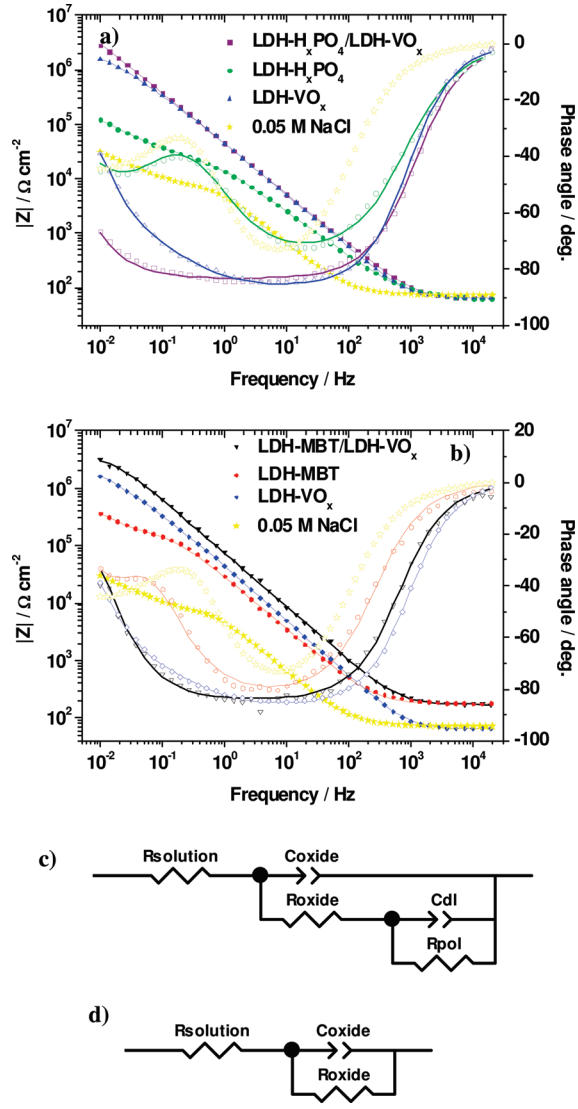

FIGURE 4. (a, b) EIs spectra obtained on AA2024 after 2 days immersion in 0.05 M NaCl doped with different LDHs; (c) equivalent circuit used for numerical modeling of spectra obtained in electrolytes with a single type of LDHs; (d) equivalent circuit used in the case of 0.05 M NaCl with combination of LDH pigments.

LDH-MBT and LDH-H_xPO_4. The middle-frequency (1×10^0 to 1×10^2 Hz) relaxation process is ascribed to the capacitance of oxide film present on the aluminum alloy surface, while the low-frequency (1×10^{-2} to 1×10^{-1} Hz) time constant is related to the undergoing corrosion activity. For the electrolyte with LDH-VO_x, the time constant associated with corrosion processes is not well pronounced, again underlining the superior inhibition of VO_x species. The impedance spectra obtained in electrolytes with combination of different LDHs (LDH-MBT/LDH-VO_x and LDH-H_xPO_4/LDH-VO_x) exhibit only one time constant originated from the native oxide film and the highest impedance values, especially in the low frequency region. This is the first evidence of a synergistic effect provided by the combination of nanocontainers loaded with different inhibitors. Although the positive combination of inhibitors H_xPO_4 and VO_x is already known in chloride media for AA2024 (14), the effectiveness of MBT/VO_x association was unknown up to now.

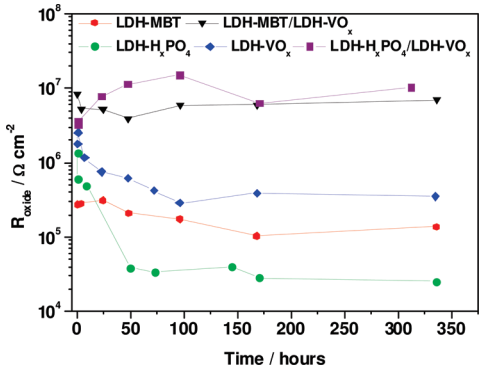

FIGURE 5. Evolution of the oxide film resistance during immersion of AA2024 in 0.05 M NaCl doped with different LDHs.

Panels c and d in Figure 4 present the electrical equivalent circuits used to fit the experimental impedance spectra recorded during immersion experiments. The equivalent circuit in panel c was used for electrolytes with individual LDH-H_xPO_4, LDH-MBT, and LDH-VO_x, whereas that in panel b was used for the combinations of LDH-MBT/LDH-VO_x and LDH-H_xPO_4/LDH-VO_x.

The oxide film on aluminum alloy is the ultimate barrier preventing direct contact between the corrosive species and the underlying metal. As a result, high oxide film resistance leads to low corrosion rate. The evolution of oxide film resistance (R_{oxide}) during immersion in different electrolytes was determined by fitting procedures using the experimental EIS data and is shown in Figure 5. Systems with individual LDHs show a rapid decrease of R_{oxide} during the first hours of immersion (most notably LDH-H_xPO_4), stabilizing after 4 days. When mixtures of LDHs are present, R_{oxide} values are the highest and remain relatively constant for the time interval monitored. Again, these results confirm the positive effect of combining different nanocontainer/inhibitor pigments.

Protective Coatings with Inhibitor-Loaded LDH Nanocontainers. Notwithstanding the positive effect of combining LDH nanocontainers loaded with different corrosion inhibitors in solution, the impact of this finding in practice is somewhat reduced because the majority of metallic substrates is not in direct contact with the environment but protected with coatings. Thus, the effect of combining different LDHs in anticorrosion coatings was surveyed using LDH-MBT and LDH-VO_x nanocontainers. MBT was selected over H_xPO_4 because MBT has shown high inhibiting properties toward AA2024 substrates in a wide pH range (35). This is important when complex systems such as multilayered coatings are used and corrosion processes can be triggered by different environmental conditions. Commercial primers used in aerospace industry were modified with LDH nanocontainers and applied to AA2024 panels, previously coated with sol–gel pretreatments (for more details see Experimental Section). In some experiments, sol–gel films were also doped with LDH-MBT. LDH-VO_x nanocontainers could not be used for the pretreatment modification because a deterioration of the sol–gel matrix was observed when vanadate was added. In a recent work (35), our group showed that MBT inhibits corrosion in bare

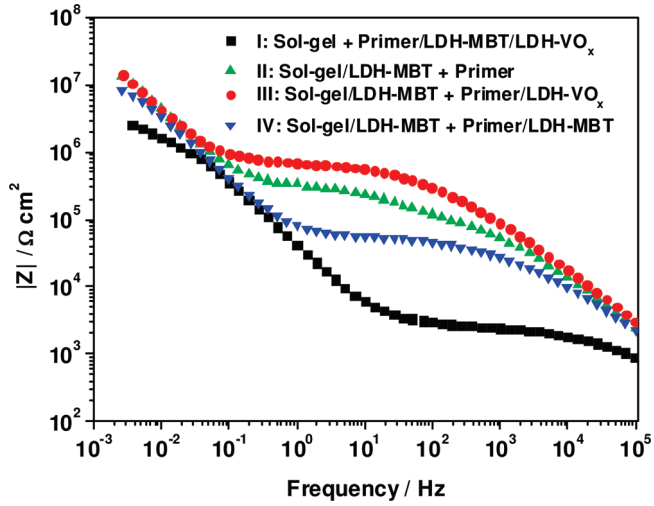

FIGURE 6. EIS spectra on AA2024 coated with different coatings taken after 30 days of immersion in 0.5 M NaCl solution.

AA2024 alloy at different pH conditions (pH 3.5, 7, 9). It is well-known that acidic conditions are generated in the head of filiform corrosion and front of the corrosion induced creapage on aluminum alloys. Therefore, an inhibitor working at low pH should be placed in the coating system as close to the metal/coating interface as possible. One could argue that the release of inhibitor from a specific nanocontainer can be negatively affected by sudden and extreme variation of conditions at the metallic interface under corrosion activity. In the case of LDHs, their structure is versatile enough to respond to such different conditions. The release of inhibitor occurs by anion-exchange, but may also be indirectly triggered by pH: at high pH levels, hydroxyl anions can be exchanged with inhibitor, whereas at very low pH levels, the LDHs dissolve acting as pH buffer and releasing inhibitor to the surroundings. The following samples were prepared and tested: **I** undoped sol–gel + primer with LDH-MBT/LDH-VO_x; **II** sol–gel with LDH-MBT + undoped primer; **III** sol–gel with LDH-MBT + primer with LDH-VO_x; **IV** sol–gel with LDH-MBT + primer with LDH-MBT. All four systems were painted with an unmodified top coat and immersed in a 0.5 M NaCl solution.

Figure 6 shows the impedance spectra after 1 month of immersion (phase angles are not shown as they do not provide additional information on coating barrier properties). The spectra reveal two time constants related to the coating properties (high frequencies) and to the properties of the oxide layer on the alloy surface (low frequencies). The calculated values of coating and oxide film resistances (R_{coat}, R_{oxide}) are presented in Table 1. The lowest resistance values were obtained for sample **I**. This demonstrates a reduction in the barrier properties of the coating system when the primer is loaded with two types of LDHs. Moreover, the absence of LDH-MBT nanocontainers on the metal/sol–gel interface explains the small R_{oxide}. Without the stabilizing action of inhibiting species the oxide film degrades relatively fast, opening access of corrosive species to the metal and leading to corrosion attack. The addition of LDH-MBT to the hybrid sol–gel layer increases the stability of the interfacial

Table 1. Electrical Parameters Obtained for Different Coatings after 30 Days of Immersion in 0.5 M NaCl

coating system	R_{coat} (Ω cm^2)	R_{oxide} (Ω cm^2)
I: sol−gel + primer/LDH-MBT/LDH-VO_x	2.83×10^3	2.52×10^6
II: sol−gel/LDH-MBT + primer	2.90×10^5	5.19×10^7
III: sol−gel/LDH-MBT + primer/LDH-VO_x	6.67×10^5	5.48×10^8
IV: sol−gel/LDH-MBT + primer/LDH-MBT	5.61×10^4	1.46×10^7

oxide film (sample **I** vs samples **II**, **III**, and **IV**); R_{oxide} is at least 6 times higher when LDH-MBT is present in the sol−gel. When LDH-MBT is additionally incorporated into the primer layer, the barrier properties of the polymer coating decrease, but at the same time the presence of these nanocontainers in the sol−gel film prevents degradation at the metal/sol−gel interface (sample **IV**). The best performance was observed for sample **III**. In this system MBT is released from the LDH nanocontainers added to the hybrid sol−gel film, stabilizing the oxide film as shown by the high values of R_{oxide}. Besides, LDH-VO_x does not lead to any significant decline of the barrier properties of the primer layer, also contributing positively to the long-term protection.

According to the aforementioned results, the positive effect of combining nanocontainers with different inhibitors in solution cannot be directly extrapolated for metal coated specimens, implying that additional parameters have to be considered. Commonly, the metallic substrates are coated with several protective layers, including pretreatment, primer, and topcoat. The midlayer (primer) is the layer where most of the active (inhibiting) species are usually incorporated, and that is why most of the samples here tested included different LDH compositions in the primer. Nonetheless, the synergistic effect observed in solution in terms of aluminum oxide stability suggests that the closeness of inhibitors to the metallic surface is more important than the combination of different LDHs farther in the primer (sample **I** vs samples **II**, **III**, and **IV**).

Furthermore, if very distinct inhibitors are used in the same coating system, only by chance do they reach the metal surface within the same time scale and concentration. Different inhibitors exhibit different solubility toward the surrounding solution and may interact with coating matrices in specific ways. For instance, the presence of LDH-MBT in the primer decreases R_{coat} (sample **IV**), whereas LDH-VO_x increases it (sample **III**). In addition, the concentration of released inhibitor from the nanocontainer can also be different (in the case of LDHs, the release is governed by an equilibrium constant) (35, 36). We suggest that the (good) performance found for coating in sample **III** offers a compromise between these parameters. At very short time scales, the interface aluminum/sol−gel film is stabilized by MBT anions, as these are the nearest available inhibiting species, whereas the long-term protection is conferred by vanadate ions released from the LDH nanoparticles present in the outer and thicker primer layer. Because the LDH-VO_x nanopigments are available in greater amounts than LDH-MBT, VO_x will protect the metallic substrate when MBT anions are no longer available. At intermediate time scales, a synergistic effect resembling that observed in solution may occur if both inhibitors are present at the interface.

Finally, some guidelines for future coating optimization can be proposed: (i) introduction of nanocontainers loaded with inhibitors into the layers closest to the metal surface such as in pretreatments; (ii) functionalization/grafting of nanocontainers to improve their interaction with the coating matrices and sustain the coating barrier properties; (iii) combination of nanocontainers in the same or in different functional layers. Regarding the importance of proximity of inhibitor-loaded nanocontainers to the metal surface, there are already some results available in the literature, indicating this trend is not limited to the nanocontainers and inhibitors here presented, or to the release mechanism associated. Recently, Abdullayev and colleagues (41) observed that sol−gel coatings doped with halloysite nanotubes, which were previously loaded with benzotriazole corrosion inhibitors, show better performances in terms of anticorrosion activity than the undoped coatings. The compatibility between nanocontainers and coating matrix, as well as the combination of different nanomaterials in the same coating, are important technical aspects to be addressed by material scientists as part of an integrated solution to potentiate the performance level of protective coatings.

CONCLUSIONS

Zn−Al LDHs intercalated with three different anionic inhibitors were synthesized by anion exchange, which emphasizes the versatility of LDH structures to incorporate different organic and inorganic anions.

The combination of LDH nanocontainers loaded with vanadate and phosphate anions, and vanadate and MBT anions, were shown to confer a synergistic anticorrosion effect on AA2024 immersed in sodium chloride solution. The inhibition effect of the LDH mixture is significantly higher than that offered by the individual systems and is attributed to stabilization of the native oxide film present on the alloy surface.

The developed nanocontainers were added to protective coatings on AA2024 with the resulting coatings showing well-defined active corrosion protection toward the AA2024 substrates. The best performance was found for the coating consisting of sol−gel film (pretreatment layer) doped with LDH-MBT and primer doped with LDH-VO_x. The interface between the aluminum alloy and sol−gel film is protected by the MBT anion available at very short time scales whereas the long-term protection is conferred by vanadate anions released from the LDH nanoparticles added to the primer. Although the potentialities of LDH nanocontainers are here highlighted for a specific coating and a metal alloy, they are worthy of further investigation as inhibiting nanomaterials for other metal alloys and coating systems.

Generically, the combination of several types of nanocontainers in the same or in different functional coating layers is a versatile route for designing active corrosion protection systems with superior performance.

Acknowledgment. This work was supported by EU FP7 project "MUST" NMP3- CP-IP 214261-2 and FCT project

PTDC/CTM/65632/2006. The authors also thank Dr. L.M. Rodrigues (Rio Grande do Sul Federal University, Brazil) for performing EIS experiments on the coated samples.

REFERENCES AND NOTES

(1) Walter, G. W. *Corros. Sci.* **1986**, *26*, 27.
(2) Koch, K.; Bhushan, B.; Ensikat, H. J.; Barthlott, W. *Philos. Trans. R. Soc, A* **2009**, *367*, 1673.
(3) Koch, K.; Ensikat, H. J. *Micron* **2008**, *39*, 759.
(4) Filipovic, N.; Kojic, M.; Tsuda, A. *Philos. Trans. R. Soc.* **2008**, *366*, 3265.
(5) *Self-Healing Materials: Fundamentals, Design Strategies, and Applications*; Ghosh, S. K., Ed.; Wiley-VCH: Weinheim, Germany, 2008.
(6) Raps, D.; Hack, T.; Wehr, J.; Zheludkevich, M. L.; Bastos, A. C.; Ferreira, M. G. S.; Nuyken, O. *Corros. Sci.* **2009**, *51*, 1012.
(7) Blustein, G.; Sarli, A. R. D.; Jaén, J. A.; Romagnoli, R.; Amo, B. D. *Corros. Sci.* **2007**, *49*, 4202.
(8) Feng, Y.; Siow, K. S.; Teo, K. T.; Hsieh, A. K. *Corros. Sci.* **1999**, *41*, 829.
(9) Rajendran, S.; Apparao, B. V.; Palaniswamy, N. *Electrochim. Acta* **1998**, *44*, 533.
(10) Feng, Y.; Siow, K. S.; Teo, W. K.; Tan, K. L.; Hsieh, A. K. *Corrosion* **1997**, *53*, 546.
(11) Birbilis, N.; Buchheit, R. G.; Ho, D. L.; Forsyth, M. *Electrochem. Solid-State Lett.* **2005**, *8*, C180.
(12) Marley, T. A.; Hughes, A. E.; Ang, T. C.; Deacon, G. B.; Junk, P.; Forsyth, M. *Electrochem. Solid-State Lett.* **2007**, *10*, C72.
(13) Forsyth, M.; Markley, T.; Ho, D.; Deacon, G. B.; Junk, P.; Hinton, B.; Hughes, A. *Corrosion* **2008**, *64*, 191.
(14) Chambers, B. D.; Taylor, S. R.; Kendig, M. W. *Corrosion* **2005**, *61*, 480.
(15) Muster, T. H.; Hughes, A. E.; Furman, S. A.; Harvey, T.; Sherman, N.; Hardin, S.; Corrigan, P.; Lau, D.; Scholes, F. H.; White, P. A.; Glenn, M.; Mardel, J.; Garcia, S. J.; Mol, J. M. C. *Electrochim. Acta* **2009**, *54*, 3402.
(16) Kallip, S. ; Bastos, A. C.; Zheludkevich, M. L.; Ferreira, M. G. S. *Corros. Sci.*, **2010**, accepted.
(17) Shchukin, D. G.; Zheludkevich, M. L.; Yasakau, K.; Lamaka, S.; Ferreira, M. G. S.; Möhwald, H. *Adv. Mater.* **2006**, *18*, 1672.
(18) Shchukin, D. G.; Zheludkevich, M. L.; Möhwald, H. *J. Mater. Chem.* **2006**, *16*, 4561.
(19) Khramov, A. N.; Voevodin, N. N.; Balbyshev, V. N.; Mantz, R. A. *Thin Solid Films* **2005**, *483*, 191.
(20) Khramov, A. N.; Voevodin, N. N.; Balbyshev, V. N.; Donley, M. S. *Thin Solid Films* **2004**, *447–448*, 549.
(21) Zheludkevich, M. L.; Serra, R.; Montemor, M. F.; Yasakau, K. A.; Salvado, I. M.; Ferreira, M. G. S. *Electrochim. Acta* **2005**, *51*, 208.
(22) Zheludkevich, M. L.; Shchukin, D. G.; Yasakau, K. A.; Möhwald, H.; Ferreira, M. G. S. *Chem. Mater.* **2007**, *19*, 402.
(23) Shchukin, D. G.; Lamaka, S. V.; Yasakau, K. A.; Zheludkevich, M. L.; Möhwald, H.; Ferreira, M. G. S. *J. Phys. Chem. C* **2008**, *112*, 958.
(24) Buchheit, R. G.; Mamidipally, S. B.; Schmutz, P.; Guan, H. *Corrosion* **2002**, *58*, 3.
(25) McMurray, H. N.; Williams, D.; Williams, G.; Worsley, D. *Corros. Eng. Sci. Technol.* **2003**, *38*, 112.
(26) Wang, H.; Presuel, F.; Kelly, R. G. *Electrochim. Acta* **2004**, *49*, 239.
(27) Buchheit, R. G.; Guan, H.; Mahajanam, S.; Wong, F. *Prog. Org. Coat.* **2003**, *47*, 174.
(28) Mahajanam, S. P. V.; Buchheit, R. G. *Corrosion* **2008**, *64*, 230.
(29) McMurray, H. N.; Williams, G. *Corrosion* **2004**, *60*, 219.
(30) Newman, S. P.; Jones, W. *New J. Chem.* **1998**, *22*, 105.
(31) Albertazzi, S.; Basile, F.; Vaccari, A. In *Clay Surfaces: Fundamentals and Applications*; Wypych, F., Satyanarayana, K. G., Eds.; Elsevier: Amsterdam, 2004; p 497.
(32) Kwak, S.-Y.; Kriven, W. M.; Wallig, M. A.; Choy, J.-H. *Biomaterials* **2004**, *25*, 5995.
(33) Williams, G.; McMurray, H. N. *Electrochem. Solid-State Lett.* **2004**, *7*, B13.
(34) Kendig, M.; Hon, M. *Electrochem. Solid-State Lett.* **2005**, *8*, B10.
(35) Poznyak, S. K.; Tedim, J.; Rodrigues, L. M.; Salak, A. N.; Zheludkevich, M. L.; Dick, L. F. P.; Ferreira, M. G. S. *ACS Appl. Mater. Interfaces* **2009**, *1*, 2353.
(36) Zheludkevich, M. L.; Poznyak, S. K.; Rodrigues, L. M.; Raps, D.; Hack, T.; Dick, L. F.; Nunes, T.; Ferreira, M. G. S. *Corros. Sci.* **2010**, *52*, 602.
(37) Barriga, C.; Jones, W.; Malet, P.; Rives, V.; Ulibarri, M. A. *Inorg. Chem.* **1998**, *37*, 1812.
(38) Gopal, R.; Calvo, C. *Acta Crystallogr., Sect. B* **1974**, *30*, 2491.
(39) Badreddine, M.; Legrouri, A.; Barroug, A.; Roy, A. D.; Bess, J. P. *Mater. Lett.* **1999**, *38*, 391.
(40) Benito, P.; Labajos, F. M.; Rocha, J.; Rives, V. *Microporous Mesoporous Mater.* **2006**, *94*, 148.
(41) Abdullayev, E.; Price, R.; Shchukin, D.; Lyov, Y. *ACS Appl. Mater. Interfaces* **2009**, *1*, 1437.

AM100174T